JOURNAL OF GUIDANCE, CONTROL, AND DYNAMICS
Vol. 26, No. 6, November–December 2003

Nondimensional Analysis of Reaction-Wheel Control for Aerobraking

Wyatt R. Johnson* and James M. Longuski†
Purdue University, West Lafayette, Indiana 47907-1282
and
Daniel T. Lyons‡
Jet Propulsion Laboratory, California Institute of Technology Pasadena, California 91109-8099

The equations of motion for an aerobraking spacecraft are nondimensionalized. This process yields three dimensionless parameters that intrinsically describe the capability of a reaction-wheel controller to manage angular momentum during an atmospheric drag pass. These parameters, namely aeromoment, desaturation speed, and equilibrium momentum, completely characterize the behavior of all reaction-wheel controllers for aerobraking at any planet. As the names imply, the behavior is determined by the density of the atmosphere, the torque of the reaction wheel, and the moment of inertia of the spacecraft (and associated parameters). Theoretical bounds on the three parameters are found, and comparisons to past aerobraking spacecraft are made. Numerical simulations demonstrate that the established bounds correctly predict the performance exhibited during aerobraking.

Nomenclature

A = system matrix
a = acceleration, m/s^2
B = input matrix
C = output matrix
C_D = coefficient of drag
C_{M_α} = derivative of spacecraft's aerodynamic moment coefficient with respect to angle of attack, deg^{-1}
c = polynomial coefficients
D^* = characteristic force ratio
d = polynomial coefficients
E = affine term
e = orbit eccentricity
g = local gravity acceleration, m/s^2
g^* = acceleration ratio
H = angular momentum, kg · m^2/s or dimensionless
I = moment of inertia, N · m
I^* = nondimensional moment of inertia
$\boldsymbol{K}$ = feedback gain matrix
M = nondimensional moment
M^* = characteristic torque ratio
m = spacecraft mass, kg
p_1 = aeromoment parameter
p_2 = desaturation speed
p_3 = reaction wheel equilibrium
q = dynamic pressure, N/m^2 or dimensionless
r = spacecraft radial distance, km or dimensionless
S = reference area, m^2
t_{char} = characteristic flythrough time, s
u = reaction wheel control torque, N · m or dimensionless
V = spacecraft velocity, km/s or dimensionless
$\boldsymbol{x}$ = state vector
α = angle of attack, deg
β = inverse scale height, km^{-1}, or sideslip angle, deg
γ = flight-path angle, deg
ΔV = change of velocity magnitude, km/s
Θ^* = atmospheric turn angle, deg
θ = true anomaly, deg
μ = gravitational parameter, km^3/s^2
ρ = atmospheric density, kg/km^3 or dimensionless
τ = nondimensional time
τ^* = relative desaturation time
Ω = inertial reaction wheel velocity, rad/s
ω = inertial spacecraft angular velocity, rad/s

Subscripts

f = final value
i = initial value
p = periapsis
rw = reaction wheel
sc = spacecraft (not including reaction wheel)

Introduction

An aerobraking spacecraft uses the atmosphere to reduce the energy of the orbit (Fig. 1). The atmospheric drag force provides the desirable ΔV to effect the orbit change. During each orbit, the spacecraft also accumulates angular momentum from several external torques, for example, aerodynamic, gravity gradient, and solar radiation pressure. Traditionally, the spacecraft reaction wheels absorb this angular momentum, allowing the spacecraft to remain in an inertial attitude. As the reaction wheels become saturated, propellant is used to eliminate the acquired angular momentum.[1] Previous aerobraking missions have used an open-loop strategy to desaturate the reaction wheels during the atmospheric drag pass.[1–3] Two major difference exist between these missions and our proposed implementation. The previous missions sequenced the desaturation maneuver relative to the predicted time of periapsis, whereas our method[4,5] senses atmospheric entry and activates a control law accordingly. The other difference is that past missions relied on attitude-control thrusters to provide attitude control during the aeropass (in the form of rate damping on the angle of attack), whereas our proposed methods rely solely on reaction wheels to achieve the same effect.

Johnson et al.[4–6] demonstrate that a reaction-wheel attitude-control law is easily capable of managing the angular momentum of a spacecraft similar (in terms of mass and aerodynamic properties)

Received 6 February 2003; revision received 9 June 2003; accepted for publication 16 June 2003. Copyright © 2003 by the authors. Published by the American Institute of Aeronautics and Astronautics, Inc., with permission. Copies of this paper may be made for personal or internal use, on condition that the copier pay the $10.00 per-copy fee to the Copyright Clearance Center, Inc., 222 Rosewood Drive, Danvers, MA 01923; include the code 0731-5090/03 $10.00 in correspondence with the CCC.

*Ph.D. Candidate, School of Aeronautics and Astronautics; currently Senior Engineer, Navigation and Mission Design, Jet Propulsion Laboratory, California Institute of Technology, 4800 Oak Grove Drive, Pasadena, CA 91109-8099. Member AIAA.

†Professor, School of Aeronautics and Astronautics. Associate Fellow AIAA.

‡Senior Engineer, Navigation and Mission Design, 4800 Oak Grove Drive.

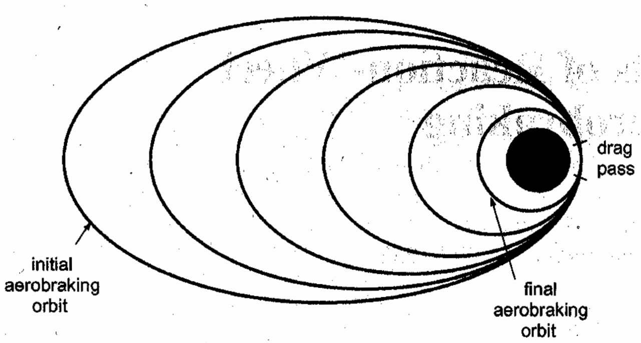

Fig. 1 Orbit decay using aerobraking.

to the Mars Global Surveyor (MGS). The performance of the previously developed control laws depends on several parameters, such as the spacecraft's inertia properties, reaction-wheel storage capacity and torque limit, and atmospheric density, to name a few. For each new aerobraking mission, a similar study would have to be performed to determine if reaction-wheel control is feasible. Similarly, if reaction-wheel control is to be used on any given mission, the spacecraft would have to be designed within some appropriate parameter space. The focus of this paper is to present specifications for the spacecraft design that determine whether or not any reaction-wheel control law is capable of managing the angular momentum in an aerobraking mission without the need for propellant-wasting reaction control.

The literature of aeroassisted maneuvers has a rich theoretical background and several applications.[2,7–13] NASA plans for regular missions to Mars at every synodic opportunity includes heavy reliance on aerobraking to reduce propellant requirements. Future missions to the atmospheric-bearing bodies in the solar system (Venus, Mars, Jupiter, Saturn, Titan, Uranus, and Neptune) will depend on aeroassisted techniques such as aerocapture, aerobraking, and aerogravity assist. In many of these cases, autonomous attitude control and momentum management will play an important role.

Nondimensionalization of the Equations of Motion

Derivation

The three axes of rotation (pitch, yaw, and roll) are dynamically coupled. However, the behavior of the aerodynamically stable axes in the six-degree-of-freedom model (pitch and yaw) indicates the single-axis model is sufficient for a feasibility study for these two axes. Thus, we will only consider the single-axis equations of motion (EOMs) and apply the results to the pitch and yaw axes independently. Angular momentum stored about the roll axis is not directly controllable. An approach to roll-axis momentum management is discussed further by Johnson et al.[14]

The dimensional orbital and momentum EOMs are given by[4,13]

$$\dot{r} = V \sin\gamma \tag{1}$$

$$\dot{V} = \frac{-qSC_D}{m} - \frac{\mu \sin\gamma}{r^2} \tag{2}$$

$$V\dot{\gamma} = -\frac{\mu \cos\gamma}{r^2} + \frac{V^2 \cos\gamma}{r} \tag{3}$$

$$\dot{\theta} = \frac{V \cos\gamma}{r} \tag{4}$$

$$\dot{\alpha} = \omega + \frac{\mu \cos\gamma}{r^2 V} \tag{5}$$

$$\dot{\omega} = \frac{\rho V^2 SLC_{M_\alpha}}{2I_{\mathrm{sc}}}\alpha - \frac{u}{I_{\mathrm{sc}}} \tag{6}$$

$$\dot{\Omega} = \frac{u}{I_{\mathrm{rw}}} \tag{7}$$

We note that the second term in Eq. (5) is due to the natural motion of the spacecraft around the planet. Because the spacecraft tends to remain in an inertially fixed attitude, the angle of attack will vary as the planet rises and falls relative to the spacecraft. This term is unique to the pitch axis.[5] The corresponding linearized yaw-axis EOM is simply

$$\dot{\beta} = \omega_{\mathrm{yaw}} \tag{8}$$

We redefine the state variables in Eqs. (6) and (7) to be the momentum instead of the angular rate, that is, $H_{\mathrm{sc}} \equiv I_{\mathrm{sc}}\omega$ and $H_{\mathrm{rw}} \equiv I_{\mathrm{rw}}\Omega$). Next, we normalize r, V, and q (dynamic pressure, given by $q = \frac{1}{2}\rho V^2$) by their values at periapsis: r_p, V_p, and q_p. Torque and angular momentum are normalized by the reaction wheel limits of $u_{\max}$ and $H_{\max}$. Finally, time is scaled by the characteristic flythrough time t_{char}[15]

$$t_{\mathrm{char}} \equiv \Delta V / a_p \tag{9}$$

$$t_{\mathrm{char}} = \sqrt{2\pi r_p^2 / \beta e \mu} \tag{10}$$

The characteristic flythrough time represents the equivalent amount of time the spacecraft is subjected to periapsis like dynamic pressures. With these normalizations, all parameters and variables for the remainder of the paper are dimensionless.

Parameterization

With these substitutions, the dimensional EOMs (1–7) become

$$\dot{r} = V \sin\gamma \cdot \Theta^* \tag{11}$$

$$\dot{V} = -g^*[q \cdot D^* + (\sin\gamma / r^2)] \tag{12}$$

$$\dot{\theta} = (V \cos\gamma / r) \cdot \Theta^* \tag{13}$$

$$\dot{\gamma} = -g^* \cdot (\cos\gamma / r^2 V) + \Theta^* \cdot (V \cos\gamma / r) \tag{14}$$

$$\dot{M} = H_{\mathrm{sc}}(M^*/I^*) + M^* g^* \cdot (\cos\gamma / r^2 V) \tag{15}$$

$$\dot{H}_{\mathrm{sc}} = -q \cdot M - (u/\tau^*) \tag{16}$$

$$\dot{H}_{\mathrm{rw}} = (u/\tau^*) \tag{17}$$

The nondimensional EOMs in Eqs. (11–17) contain six nondimensional parameters that are defined in Table 1.

An orbit shape is characterized by two parameters, for example, semimajor axis and eccentricity. In our nondimensional parameterization, the orbit is characterized by Θ^* (the atmospheric turn angle) and g^* (an acceleration ratio). The third parameter D^* describes the drag force. The three remaining parameters pertain to the momentum EOMs (15–17).

Two terms produce coupling between the orbital EOMs and the momentum EOMs. The first occurs in the last term of Eq. (15), due to the presence of γ, r, and V. We note that near periapsis (the area of interest for aerobraking), this last term is approximately unity. The second source of coupling is implicit from the q term of Eq. (16). Because of our choice of time scaling, $q \approx 0$ for $|t| > 1$ and $q = 1$ for $t = 0$. The exact shape of $q(t)$ is dependent on the orbit eccentricity. From our earlier definitions, however, $q \approx 1$ over one timescale. Thus, the differences in shape should be fairly minor.

Table 1 Nondimensional parameters

Parameter	Definition	Description
Θ^*	$V_p t_{\mathrm{char}}/r_p$	Atmospheric turn angle
g^*	$(\mu/r_p^2)/(V_p/t_{\mathrm{char}})$	Acceleration ratio
D^*	$(q_p SC_D/m)/(\mu/r_p^2)$	Characteristic force ratio
M^*	$-q_p SLC_{M_\alpha}/(H_{\max}/t_{\mathrm{char}})$	Characteristic torque ratio
I^*	$I/(H_{\max} t_{\mathrm{char}})$	Nondimensional moment of inertia
τ^*	$(H_{\max}/u_{\max})/t_{\mathrm{char}}$	Relative desaturation time

Table 2 Reduced nondimensional parameters

Parameter	Definition	Description
p_1	$\sqrt{M^*/I^*}$	Aeromoment
p_2	$1/\tau^*$	Desaturation speed
p_3	I^*g^*	Equilibrium momentum

With these assumptions, we can decouple the momentum EOMs from the orbital EOMs and analyze the structure of the momentum EOMs independently. The approximate EOMs inside the atmosphere are, thus, given by the linear time-varying system:

$$\dot{M} = H_{sc}(M^*/I^*) + M^*g^* \tag{18}$$

$$\dot{H}_{sc} = -q \cdot M - (u/\tau^*) \tag{19}$$

$$\dot{H}_{rw} = (u/\tau^*) \tag{20}$$

For convenience, we make the following definitions and approximation:

$$p_1 \equiv \sqrt{M^*/I^*} \tag{21}$$

$$p_2 \equiv 1/\tau^* \tag{22}$$

$$p_3 \equiv I^*g^* \tag{23}$$

$$q(t) \approx 1 \tag{24}$$

The approximation in Eq. (24) is made to simplify the EOMs into a linear time-invariant system. This approximation is accurate near periapsis, that is, during the time the controller is active. Our final form of the nondimensional momentum EOMs is thus,

$$\dot{M} = H_{sc}p_1^2 + p_1^2 p_3(\cos\gamma/r^2V) \tag{25}$$

$$\dot{H}_{sc} = M - up_2 \tag{26}$$

$$\dot{H}_{rw} = up_2 \tag{27}$$

The new nondimensional parameters p_1, p_2, and p_3 (Table 2) have the following physical interpretations:

1) Parameter p_1 is the aeromoment parameter. It describes the atmosphere's ability to rotate the spacecraft. Larger p_1 values correspond to more dense atmospheres.

2) Parameter p_2 is the desaturation speed of the reaction wheel. A large p_2 means the reaction wheel is capable of despinning (spinning down from its initial speed to zero) quickly.

3) Parameter p_3 is the equilibrium momentum for the pitch axis. The equilibrium for the spacecraft momentum is $-p_3$, and for the reaction wheel, it is $+p_3$ (when the total system momentum is zero). The sideslip angle β has a zero equilibrium value, and thus, we let $p_3 = 0$ for this special case. By definition of p_3, we have the constraint that

$$0 \leq p_3 \leq 1 \tag{28}$$

The linear system can be written as

$$\dot{x} = Ax + Bu + E \tag{29}$$

$$H = Cx \tag{30}$$

where

$$x = [M \quad H_{sc} \quad H_{rw}]^T \tag{31}$$

$$A = \begin{bmatrix} 0 & p_1^2 & 0 \\ -1 & 0 & 0 \\ 0 & 0 & 0 \end{bmatrix} \tag{32}$$

$$B = [0 \quad -p_2 \quad p_2]^T \tag{33}$$

$$C = [0 \quad 1 \quad 1] \tag{34}$$

$$E = \left[p_1^2 p_3 \quad 0 \quad 0\right]^T \tag{35}$$

Evolution of Parameters

The parameters p_1, p_2, and p_3 are not constants, but rather they evolve over time. The first two parameters are both directly proportional to t_{char}, which increases as the orbit decays. The smallest values of p_1 and p_2 will, thus, occur on the initial orbit, when orbit period is greatest. For a particular control law, the performance will depend on the spacecraft design, the reaction wheels, and atmospheric properties. The most restrictive case is the initial aerobraking pass, where flythrough time is short: The controller's performance will generally improve on subsequent orbits.

If the initial and final orbit eccentricities are known, the ratio of the final value of p_1 or p_2 to its initial value can easily be computed. For example, MGS captured into a 48-h elliptical orbit ($e \approx 0.9$), and it completed its last aerobraking orbit once it reached a 2-h orbit ($e \approx 0.1$):

$$p_f/p_i = \sqrt{e_i/e_f} = \sqrt{0.9/0.1} = 3 \tag{36}$$

$$\log_{10}p_f - \log_{10}p_i = \log_{10}3 \approx 0.5 \tag{37}$$

The p_3 parameter is inversely proportional to $r_p^2V_p$. Periapsis distance will vary significantly less than periapsis velocity. Thus, the ratio of $p_{3,f}$ to $p_{3,i}$ is found by

$$p_f/p_i = r_i^2 V_i \big/ r_f^2 V_f \tag{38}$$

$$p_f/p_i \approx V_i/V_f = \sqrt{(1+e_i)/(1+e_f)} \approx 1.31 \tag{39}$$

$$\log_{10}p_f - \log_{10}p_i \approx 0.12 \tag{40}$$

Thus, $\log_{10}p_1$ and $\log_{10}p_2$ can be expected to increase by about 0.5 over the course of a mission, whereas $\log_{10}p_3$ increases by about 0.12.

Typical Parameters

Table 3 lists dimensional data[2,3,10,11,16–18] and the derived nondimensional parameters for three aerobraking spacecraft: Magellan, MGS, and a hypothetical aerocapture tether.

Magellan's initial aerobraking orbit was at $e = 0.39$, whereas MGS began aerobraking at $e = 0.9$. To present a fair comparison between the spacecraft, an eccentricity of 0.9 is used. (The p_1 and p_2 values for the initial Magellan aerobraking orbit are roughly 50% greater than listed in Table 3.) The tether case uses an eccentricity of 1.54 (which corresponds to the Hohmann transfer) because this is an aerocapture example.

As we shall see, the determining factors in momentum control during aerobraking are the p_1 and p_2 parameters. Reaction-wheel control is only suitable for spacecraft with $p_1 \gg 2$. Magellan and MGS both meet this requirement in the extreme case of $e = 0.9$, whereas the tether does not. MGS exceeds this threshold by a much greater margin than Magellan, but MGS was designed to aerobrake, whereas Magellan was not.

Control Laws

We consider three atmospheric control laws. An inertial attitude hold mode is used until the spacecraft descends through the sensible atmosphere at $t = -1$, at which time, an atmospheric controller is activated. At atmospheric exit, any residual angular momentum is reabsorbed by the reaction wheels, and normal exoatmospheric attitude control resumes. The three control laws we examine are the spin down, the affine partial state, and the two stage.[4,5] First, we analyze the natural behavior of the system when control is not applied.

Table 3 Nondimensional parameters for three spacecraft

	Magellan		MGS		
Parameter	Pitch	Yaw	Pitch	Yaw	Hypothetical tether[a]
e	0.9[b]	0.9[b]	0.9	0.9	1.54
β, 1/km	0.167	0.167	0.145	0.145	0.125
μ, km^3/s^2	324,859	324,859	42,828	42,828	42,828
r_p, km	6,189.3	6,189.3	3,514	3,514	3,490
t_{char}, s	70.3	70.3	117.8	117.8	95.4
m, kg	1,100	1,100	760	760	2,112
S, m^2	22.7	22.7	17.04	17.04	605
L, m	3.7	3.7	8.73	8.73	7,250
q_p, N/m^2	0.27	0.27	0.18	0.18	7.3
C_D	2.2	2.2	1.95	1.95	1.0
C_{M_α}, 1/rad	−0.48	−0.57	−0.21	−0.57	−1.0
I, km · m^2	2,209	1,204	410	814	1.07×10^{11}
$H_{\max}$, km · m^2/s	27	27	22	22	N/A
$u_{\max}$, km · m^2/s^2	0.18	0.18	0.14	0.14	N/A
Θ^*	0.113	0.113	0.161	0.161	0.154
g^*	0.060	0.060	0.085	0.085	0.060
D^*	0.00145	0.00145	0.00227	0.00227	0.591
M^*	28.22	33.86	30.13	82.18	N/A
I^*	1.16	0.63	0.16	0.31	N/A
τ^*	2.13	2.13	1.33	1.33	N/A
p_1	4.92	7.30	13.8	16.2	1.64[c]
p_2	0.47	0.47	0.75	0.75	N/A
p_3	0.069	0[d]	0.013	0[d]	N/A
$\log_{10} p_1$	0.69	0.86	1.14	1.21	0.22
$\log_{10} p_2$	−0.33	−0.33	−0.12	−0.12	N/A
$\log_{10} p_3$	−1.16	$-\infty$	−1.87	$-\infty$	N/A

[a] Tether example does not have reaction wheels; thus corresponding parameters are not applicable.

[b] Magellan began aerobraking at $e = 0.39$; data are presented for $e = 0.9$ to allow comparison to MGS.

[c] M^*/I^* is defined even though M^* and I^* are not defined individually.

[d] For the yaw axes $p_3 \equiv 0$

No Control

We can gain insight into the behavior of the system by first considering the case of no control. In this case, the reaction wheel is held at constant speed when the spacecraft enters the atmosphere, and thus, $u = 0$. The open-loop eigenvalues are easily seen to be

$$\lambda = \{0, \pm \jmath p_1\} \tag{41}$$

The oscillations in the spacecraft's attitude are therefore, undamped with a (nondimensional) frequency of p_1 radian. Thus, the instantaneous period of a single oscillation in the spacecraft's attitude should be $2\pi/(\sqrt{(q)}p_1)$. The shortest period occurs at periapsis, where $q = 1$. Away from periapsis, the period of oscillation is longer. The average period of oscillation (during the aerobraking pass) is, thus, larger, numerically found to be roughly $8/p_1$. Because the sensible atmosphere spans about two time units, the spacecraft oscillates through at least one full cycle when $p_1 \geq 4$. A half-cycle deflection yields the worst performance, because the resulting angle-of-attack history is maximally biased. (The spacecraft's angle of attack reaches a maximum at periapsis.) For this reason, the region near $p_1 = 2$ presents the most challenging control problem, because a reaction-wheel controller needs at least a full period to damp out angle-of-attack oscillations, or only a fraction of a period to use a passive momentum management scheme.

As indicated earlier, Magellan and MGS are both in the $p_1 \gg 2$ region (and thus, reaction-wheel control is feasible for these spacecraft), but the tether is not (because $p_1 = 1.64 < 2$). The best approach for momentum control of the aerobraking tether is to follow the passive scheme.[16]

Spin Down

The spin-down controller applies maximum torque to the reaction wheel when the spacecraft is near periapsis. This mechanism is possible because the spacecraft can torque against the atmosphere, which tends to keep the spacecraft from rotating, while the wheels are desaturated. The spin-down control law works best if started near periapsis, where the atmosphere is densest. In terms of the nondimensional variables, the time required to spin down a reaction wheel with stored momentum H_{rw} is simply H_{rw}/p_2. The control law is activated at $t = -H_{\mathrm{rw}}/2p_2$ so that the spin down will be halfway complete at periapsis.

We can immediately place a lower bound of the value of p_2. The actual atmospheric flythrough time is approximately two timescales ($2t_{\mathrm{char}}$). The spin-down operation must take place within the atmosphere, and so we have the constraint that

$$H_{\mathrm{rw}}/p_2 < 1/p_2 < 2 \tag{42}$$

This leads us to identify a critical value $p_{2,\mathrm{crit}}$, such that

$$p_2 > p_{2,\mathrm{crit}} = \tfrac{1}{2} \tag{43}$$

This constraint states that the reaction wheel must be capable of desaturating within the sensible atmosphere. From Table 3, we see that MGS meets this requirement for all orbits. Magellan is slightly below this threshold for the $e = 0.9$ case but meets the requirement for its initial aerobraking orbit (where $p_2 = 0.7$).

Affine Partial State

The affine partial-state controller uses feedback from the two measurable state variables, H_{sc} and H_{rw}. Without the ability to measure the third state variable M, the closed-loop system poles cannot be arbitrarily placed. Furthermore, the system is time varying so that negative eigenvalues are insufficient for closed-loop stability. We take the approach of finding the feedback gain vector, $\boldsymbol{K} = [0 \quad K_{\mathrm{sc}} \quad K_{\mathrm{rw}}]$, to minimize the maximum real component of the eigenvalues.

For any monic polynomial with exactly one specified coefficient, the minimax solution occurs when the roots are real and identical.

Proof by Contradiction

Consider the monic polynomial, $c_n = 1$, given by

$$p(s) = \sum_{k=0}^{n} \binom{n}{k} c_k^{n-k} s^k \tag{44}$$

If the jth term is the only specified term, then the minimax solution is given by $c_k = c_j$ for all k, which yields

$$p_j(s) = \sum_{k=0}^{n} \binom{n}{k} c_j^{n-k} s^k \tag{45}$$

$$p_j(s) = (s + c_j)^n \tag{46}$$

Let us assume that $p_j(s)$ is not the minimax solution. In other words, every root of $p(s)$ has a real part smaller than c_j. We will call this better polynomial $q(s)$

$$q(s) = \sum_{k=0}^{n} \binom{n}{k} d_k^{n-k} s^k \tag{47}$$

$$q(s) = \prod_{i=1}^{n} (s + c_j + \epsilon_i) \tag{48}$$

Our constraints are that $d_j = c_j$ (the jth term is fixed), and $\Re\{\epsilon_i\} > 0$ for all i. [We need every root of $q(s)$ to be smaller than c_j.] Expansion of Eq. (48) reveals that

$$\binom{n}{j} d_j^{n-j} = \sum_{k=1}^{\binom{n}{j}} \prod_{i=1}^{n-j} (c_j + \epsilon_{k_i}) \tag{49}$$

$$\binom{n}{j} d_j^{n-j} > \binom{n}{j} c_j^{n-j} \tag{50}$$

$$d_j > c_j \tag{51}$$

However, our original assumption was that $d_j = c_j$, that is, the jth term was fixed, and so we have a contradiction. Therefore, if any term in a polynomial has exactly one coefficient that is fixed, with the rest arbitrary, then the polynomial that minimizes the maximum real part of the roots is the polynomial with n repeated real roots.

Application to the Affine Partial State Controller

The characteristic polynomial for the closed-loop system is

$$s^3 + s^2 p_2(K_{\mathrm{sc}} - K_{\mathrm{rw}}) + s p_1^2 - K_{\mathrm{rw}} p_1^2 p_2 = 0 \qquad (52)$$

In Eq. (52), the s term has a fixed coefficient (no feedback available). Because the s term is the only such term, we know the minimax solution occurs when all roots are real and identical. From Eq. (52), we deduce the (triple-root) closed-loop eigenvalue to be

$$s = -p_1/\sqrt{3} \qquad (53)$$

The required feedback coefficients are given by

$$K_{\mathrm{sc}} = 8p_1 \big/ \sqrt{27} p_2 \qquad (54)$$

$$K_{\mathrm{rw}} = -p_1 \big/ \sqrt{27} p_2 \qquad (55)$$

One important result from picking gain values proportional to p_1/p_2 is that the desaturation parameter p_2 scales out of the characteristic polynomial. In other words, as long as the constraint Eq. (43) holds, the system performance is independent of the reaction wheel size.

The optimal feedback parameters are functions of atmospheric parameters, which may not be known very precisely and could substantially differ from orbit to orbit. We have found this control approach to be very robust, even with orbit-to-orbit density variations ranging from 10 to 200% of nominal values. The robustness is discussed in further detail by Johnson et al.[6,14]

Two Stage

The affine partial-state controller works best when started early during the drag pass, and the spin down controller works best near periapsis. The two-stage controller combines the affine partial-state and spin-down controllers.[4,5]

Results

There are three significant control strategies, based on the aeromoment parameter. For sufficiently large p_1, a reaction-wheel control law is capable of controlling the attitude while dumping the system angular momentum.[4,5] This active control operates best when the angle-of-attack oscillations have a small amplitude. The entry angle of attack is chosen to minimize this amplitude.

When the aeromoment is too small, a reaction-wheel controller does not have enough time per drag pass to dump all of the system momentum. However, a specific entry attitude can yield the desired ΔH. This passive-control strategy of targeting for a particular entry attitude applies when the spacecraft's attitude oscillates through a fraction of a period (and is thus predictable).

We can also employ both techniques to achieve a more robust controller. An entry attitude is selected such that the natural oscillations of the spacecraft should result in zero system momentum after the drag pass. For high p_1, this entry-attitude scheme is virtually impossible because any perturbation on the atmospheric density would ruin the estimate. Once atmospheric entry is detected, reaction-wheel control is used to dump angular momentum actively. However, for low p_1, this dumping scheme is ineffective because of insufficient time. As we shall see, a composite strategy accommodates systems for arbitrary values of p_1, that is, from very low to very high.

Case 1: High Aeromoment (Active Control)

Figure 2 shows the fractional momentum remaining after a drag pass using the spin-down controller over a range of p_1 and p_2 values. The blue regions indicate no angular momentum is remaining after a pass, whereas a red region indicates the final momentum is at least 100% of reaction wheel capacity. The reaction wheel is initially fully saturated (arbitrarily in the positive direction). We allow the reaction wheel to be saturated initially to maximum capacity to demonstrate the worst-case performance. A wheel with leftover margin would behave at least as well as a smaller wheel with no margin, that is, by a simple rescaling of the nondimensional parameters. (The performance will not necessarily be identical because of the inherent nonlinearity of saturation.)

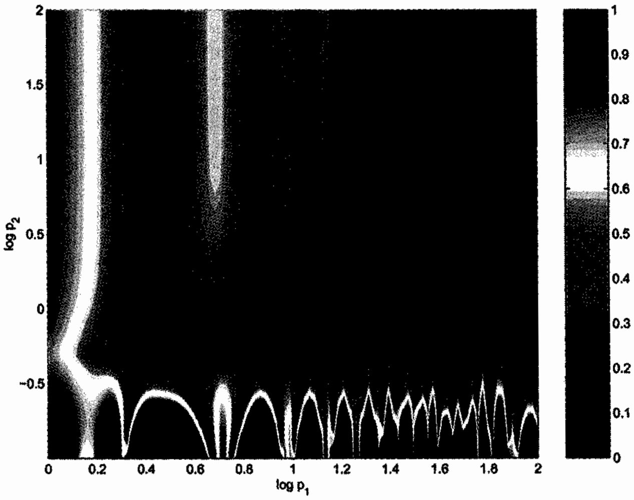

Fig. 2 Fractional momentum remaining after a drag pass using spin-down controller: horizontal axis provides the aeromoment (atmospheric density), vertical axis provides the desaturation speed (reaction-wheel strength), blue regions indicate greatest reduction of angular momentum, and red regions indicate insufficient dumping.

As predicted earlier, there are minimum values of p_1 and p_2 for which the control law works. When a log scale is used, the predicted constraints for feasible control are $\log_{10} p_1 > 0.3$ and $\log_{10} p_2 > -0.3$. However, the spin-down controller can suffer if p_2/p_1 exceeds some threshold. If p_2 is large, the reaction wheel despins too quickly. The net result is that the spacecraft's attitude is mostly uncontrolled because no control is used before or after the desaturation. Whereas the natural oscillations in the spacecraft will tend to pick up additional momentum, the initial bias is removed. Because a weaker reaction wheel performs better in this case than a stronger reaction wheel, the control law can easily be modified by reducing the torque to prolong the spin-down duration.

The control law performance near the critical p_2 threshold is coincidentally due to a fortunate initial condition in the angle of attack. In some of the cases, the entry angle of attack is such that the net angular momentum accumulation is destructive, and the final system momentum is low. In the remaining cases, the net angular momentum accumulation is constructive, and the final system momentum is even larger. Because a small perturbation in the atmospheric density profile can shift the locations of these waves, we cannot use this effect to our advantage. This limitation is inherent to the high p_1 case, as will be shown later.

The affine partial-state controller (Fig. 3) performs noticeably better than the spin down. This controller is able to operate in a lower p_2 range than the spin down can and has more consistent behavior at low p_1. Furthermore, the closed-loop eigenvalues [Eq. (53)] are solely a function of p_1 as the results in Fig. 3 confirm for $\log_{10} p_2 > \log_{10} p_{2,\mathrm{crit}} = -0.3$. There is a slight gradient in the p_2 direction, however. Equation (53) was derived from idealized assumptions that ignore the reaction-wheel torque limit. In the low p_2 cases, the reaction-wheel torque saturates, and thus, the commanded torque is less than the requested torque. For high p_2, the requested torque is available. One important difference between the affine partial-state and spin-down controllers is that the former improves with increasing p_2, whereas the latter worsens.

The two-stage controller (Fig. 4) is the best out of the three considered laws. At first glance at Fig. 4 we notice that the lightly shaded

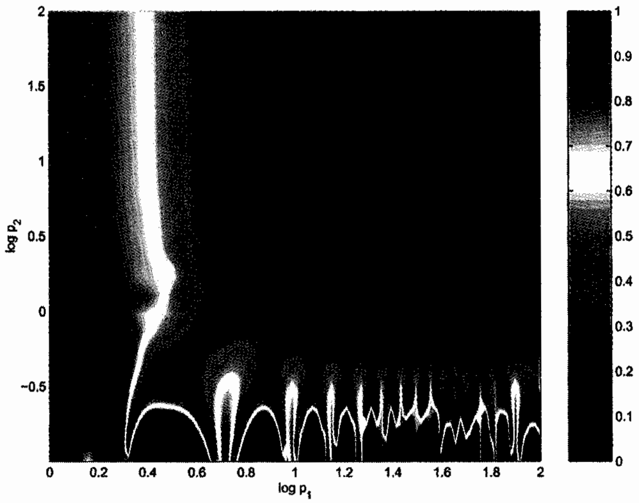

Fig. 3 Fractional momentum remaining after a drag pass using affine partial-state controller.

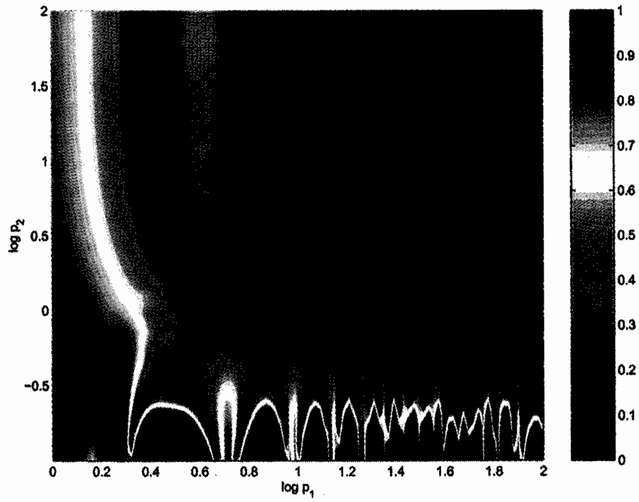

Fig. 4 Fractional momentum remaining after a drag pass using two-stage controller.

regions are greater in area than for the other two control laws. From a practical consideration, the two-stage controller is also less sensitive to periapsis timing errors[4,5] than the spin-down controller while still maintaining the advantage of the affine partial-state controller. These aspects make the two-stage controller the most robust of the three considered control laws.

Case 2: Low Aeromoment (Passive Control)

For low p_1, the atmospheric density is too thin (or the spacecraft is too massive) for the atmosphere to deflect the spacecraft's attitude significantly. In this case, we can make the approximation that $\dot{H}_{sc} = 0$. Equation (25) can be solved:

$$\dot{M} = H_{sc} p_1^2 + p_1^2 p_3 (\cos\gamma / r^2 V) \approx p_1^2 (H_{sc} + p_3) \qquad (56)$$

$$M(t) = M(t_0) + p_1^2 [H_{sc}(t_0) + p_3](t - t_0) \qquad (57)$$

Thus, the angle of attack grows linearly in the vicinity of periapsis. With this solution to the time history of $M(t)$ (and a few more assumptions), we can calculate the angular impulse the spacecraft receives at periapsis and use this information to select the proper entry attitude to remove passively the spacecraft's angular momentum.

When no control is used, Eq. (26) becomes

$$\dot{H}_{sc} = -q \cdot M \qquad (58)$$

Integrating Eq. (58) over the drag pass will yield the ΔH. Let the atmosphere be modeled by the (nondimensional) exponential density law:

$$\rho = \exp[-\beta r_p (r - 1)] \qquad (59)$$

From Table 1, we have that

$$\Theta^* = \frac{V_p t_{\mathrm{char}}}{r_p} \qquad (60)$$

$$\Theta^* = \sqrt{\frac{\mu(1+e) 2\pi r_p^2}{\beta r_p^3 e \mu}} \qquad (61)$$

Thus,

$$\Theta^{*2} = \frac{2\pi(1+e)}{\beta r_p e} \qquad (62)$$

so that

$$\beta r_p = \frac{2\pi(1+e)}{\Theta^{*2} e} \qquad (63)$$

Substituting Eq. (63) into Eq. (59) yields

$$\rho = \exp\left[\frac{-2\pi(1+e)(r-1)}{\Theta^{*2} e}\right] \qquad (64)$$

The aerodynamic moment will be proportional to q, which must be integrated over the entire drag pass. Because the density changes much faster than the velocity, we can approximate the velocity as a constant over the orbit. To integrate q over the entire orbit, we need to express the term $r - 1$ in Eq. (64) in a more convenient fashion.[15] We approximate it with a Taylor series in powers of true anomaly θ, noting that, because $r - 1$ is an even function, then only even powers of θ will be present in the expansion.

Thus, the nondimensional dynamic pressure is found to be

$$q = \rho V^2 \approx \exp\left[\frac{-2\pi(1+e)(r-1)}{\Theta^{*2} e}\right] \qquad (65)$$

and the nondimensional altitude is obtained from

$$r - 1 = \frac{1+e}{1+e\cos\theta} - 1 = \frac{e - e\cos\theta}{1+e\cos\theta} \qquad (66)$$

$$r - 1 = e\left[0 + 0\theta + \frac{1}{2(1+e)}\theta^2 + \cdots\right] = \frac{e\theta^2}{2(1+e)} \qquad (67)$$

Combining Eqs. (65) and (67) yields

$$q = \exp\left[-\pi(\theta/\Theta^*)^2\right] \qquad (68)$$

From the angular momentum EOM

$$\dot{H}_{sc} = -q \cdot M = -q \cdot \left[M(0) + p_1^2 (H_{sc} + p_3) t\right] \qquad (69)$$

We can write [with the help of Eqs. (13), (69), and (68)]

$$\frac{\mathrm{d}H}{\mathrm{d}\theta} = \frac{\dot{H}}{\mathrm{d}\theta/\mathrm{d}\tau}$$

$$\frac{\mathrm{d}H}{\mathrm{d}\theta} = -\frac{M(0) + p_1^2 (H_{sc} + p_3) t}{\Theta^*} \exp\left[-\pi\left(\frac{\theta}{\Theta^*}\right)^2\right] \qquad (70)$$

At apoapsis, the atmospheric density is negligible (for moderate to high eccentricities). The form of Eq. (70) has a simple closed-form solution if we extend the limits of integration to ±∞. A true anomaly in the added range has no physical meaning, that is, our density function is not periodic, but because the atmospheric density is negligible in this realm anyway, the error in using this approximation is small. Furthermore, Eq. (70) is the sum of an even function and an odd function. The integral of the odd function over $\pm\infty$ is zero. Finally, the impulsive ΔH is given by

$$\Delta H = -\int_{-\infty}^{\infty} \frac{M(0)}{\Theta^*} \exp\left[-\pi\left(\frac{\theta}{\Theta^*}\right)^2\right] \mathrm{d}\theta \tag{71}$$

$$\Delta H = -M(0) \tag{72}$$

The passive momentum management strategy is, thus, to target the inertial attitude such that the normalized angle of attack at periapsis is equal and opposite in magnitude to the stored momentum. This strategy is used by Longuski et al.[16] for aerobraking tethers. For the low p_1 case, atmospheric perturbations will not significantly disturb the spacecraft's attitude. Thus, we can propogate the desired angle of attack at periapsis backward to the entry condition.

Figure 5 illustrates the final momentum after a drag pass using passive control. As with the earlier cases, the initial reaction wheel saturation is 100%. A reaction wheel is still used to maintain an inertial attitude before atmospheric entry, and thus, Fig. 5 is a function of both p_1 and p_2. However, the performance of the passive-control method is largely independent of p_2 in the low p_1 regime. As we can see from Fig. 5, the region for which the passive control is designed ($\log_{10} p_1 \ll 0.3$) is predominantly blue, which indicates that most of the angular momentum is dumped.

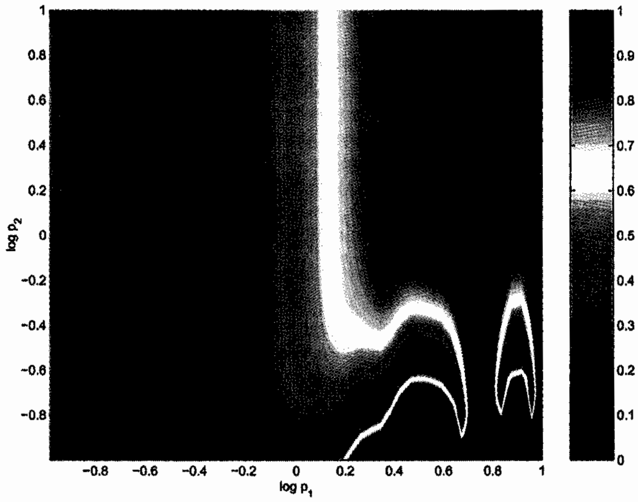

Fig. 5 Fractional momentum remaining after a drag pass using passive control.

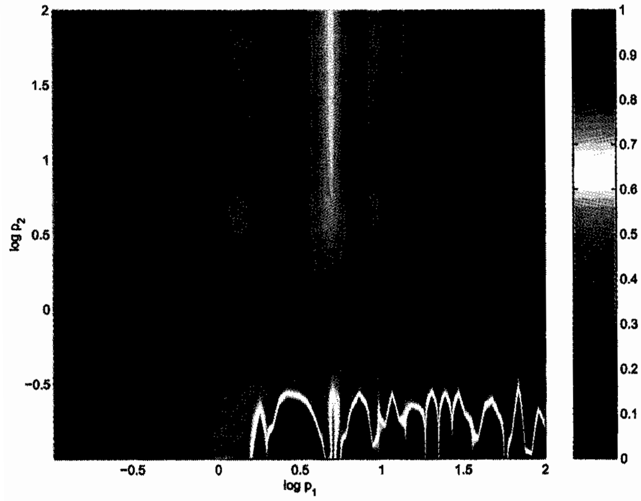

Fig. 6 Fractional momentum remaining after a drag pass using spin-down controller.

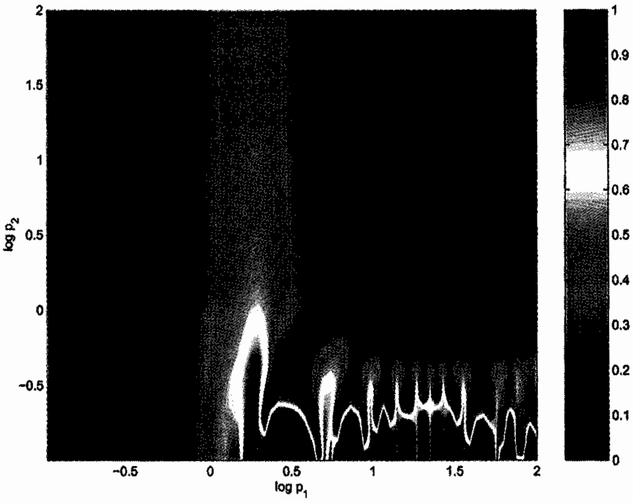

Fig. 7 Fractional momentum remaining after a drag pass using affine partial-state controller.

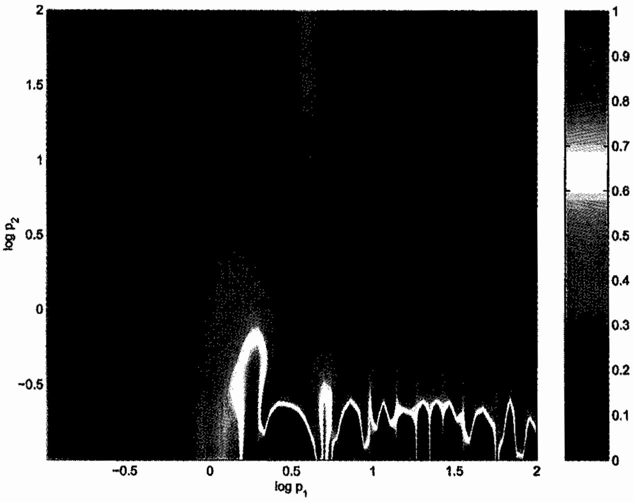

Fig. 8 Fractional momentum remaining after a drag pass using two-stage controller.

Case 3: Composite Strategy

We now combine the active- and passive-control strategies to yield a method that is appropriate for any value of p_1. The entry attitude is chosen to remove passively the stored momentum, and a reaction-wheel control law is used during the flythrough. The difference in selected entry attitude will be irrelevant for high p_1 because a reaction-wheel controller is much more insensitive to entry conditions in this realm. The results for this case are presented in Figs. 6–8. In these cases, the performance in the high p_1 portion is nearly identical to the earlier results in Figs. 2–4. The composite strategy extends the reaction-wheel control capabilities into the low p_1 regime, as well as into the difficult to control intermediate p_1 regime ($p_1 \approx 2$).

Conclusions

The nondimensional analysis reveals three parameters that determine control law performance. The first of these is the aeromoment parameter, which is a function of atmospheric and aerodynamic properties. The second is the desaturation speed parameter, which describes the relative strength of the reaction wheel. The third is the reaction-wheel equilibrium parameter, which is a function of gravitational and moment-of-inertia properties.

Theoretical limits (which are controller-independent) are derived for the three parameters. In all cases, the reaction wheel must be capable of desaturation within the atmosphere, and the reaction-wheel equilibrium momentum must be within the reaction-wheel limits. For active control, the aeromoment should be large enough for oscillations in attitude to occur. For passive control, the aeromoment should be very small to allow accurate predictions of angular impulse. These limits are necessary (but not sufficient) conditions for suitable performance.

Three reaction-wheel control laws are considered: spin down, affine partial state, and the two stage. Numerical simulations indicate that the theoretical limits are necessary and sufficient conditions for the affine partial-state and two-stage controllers. However, the spin-down controller has an additional constraint in that the reaction-wheel strength cannot be too large. By contrast, the affine partial-state and two-stage controllers perform better with increasing reaction-wheel strength.

In general, these analytic results determine limits on the design of spacecraft attitude-control systems to be used in aeroassisted missions. The three characteristic parameters provide specific guidelines for missions at any of the atmosphere-bearing bodies in the solar system.

Acknowledgments

This work was funded in part by the Purdue Research Foundation and the Jet Propulsion Laboratory (JPL), California Institute of Technology, Pasadena, California, under JPL Contract 1223406 (G. T. Rosalia, Contract Manager and Dennis V. Byrnes, Technical Manager). Portions of the work described were performed at JPL, California Institute of Technology, under contract with NASA.

References

[1] Lyons, D., "Aerobraking Automation Options," *AAS/AIAA Astrodynamics Conference*, Vol. 109, Pt. 2, edited by D. B. Spencer, C. C. Seybold, A. K. Misra, and R. J. Lisowski, Univelt, San Diego, CA, 2002, pp. 1231–1246.

[2] Lyons, D., "Aerobraking at Venus and Mars, a Comparison of the Magellan and Mars Global Surveyor Aerobraking Phases," *AAS/AIAA Astrodynamics Conference*, Vol. 103, Pt. 1, edited by K. C. Howell, F. R. Hoots, B. Kaufman, and K. T. Alfriend, Univelt, San Diego, CA, 2000, pp. 859–878.

[3] Carpenter, A., and Dukes, E., "Control of the Magellan Spacecraft During Atmospheric Drag," *Guidance and Control 1994*, edited by R. D. Culp and R. D. Rausch, Univelt, San Diego, CA, 1994, pp. 533–554.

[4] Johnson, W., Longuski, J., and Lyons, D., "Attitude Control During Autonomous Aerobraking for Near-Term Mars Exploration," *AAS/AIAA Astrodynamics Conference*, Vol. 109, Pt. 2, edited by D. B. Spencer, C. C. Seybold, A. K. Misra, and R. J. Lisowski, Univelt, San Diego, CA, 2002, pp. 1273–1292.

[5] Johnson, W., Longuski, J., and Lyons, D., "High-Fidelity Modeling of Semi-Autonomous Attitude Control During Aerobraking," AIAA Paper 2002-4909, Aug. 2002.

[6] Johnson, W. R., Longuski, J. M., and Lyons, D. T., "Pitch Control During Autonomous Aerobraking for Near-Term Mars Exploration," *Journal of Spacecraft and Rockets*, Vol. 40, No. 3, 2003, pp. 371–379.

[7] Munk, M., and Powell, R., "Aeroassist Technology Planning for Exploration," *AAS/AIAA Spaceflight Mechanics Meeting*, Vol. 105, Pt. 2, edited by C. A. Kluever, B. Neta, C. D. Hall, and J. M. Hanson, Univelt, San Diego, CA, 2000, pp. 1073–1084.

[8] Spencer, D., and Braun, R., "Mars Pathfinder Atmospheric Entry: Trajectory Design and Dispersion Analysis," *Journal of Spacecraft and Rockets*, Vol. 33, No. 5, 1996, pp. 670–676.

[9] Lyons, D., Beerer, J., Esposito, P., Johnston, M., and Willcockson, W., "Mars Global Surveyor: Aerobraking Mission Overview," *Journal of Spacecraft and Rockets*, Vol. 36, No. 3, 1999, pp. 307–313.

[10] Wilmoth, R. G., Rault, D. F., Cheatwood, F. M., Engelund, W. C., and Shane, R. W., "Rarefied Aerothermodynamic Predictions for Mars Global Surveyor," *Journal of Spacecraft and Rockets*, Vol. 36, No. 3, 1999, pp. 314–322.

[11] Lyons, D., "Aerobraking Magellan: Plan Versus Reality," *AAS/AIAA Spaceflight Mechanics Meeting*, Vol. 87, Pt. 2, edited by J. E. Cochran Jr., C. D. Edwards Jr., S. J. Hoffman, and R. Holdaway, Univelt, San Diego, CA, 1994, pp. 663–680.

[12] Tragesser, S., and Longuski, J., "Analysis and Design of Aerocapture Tether with Accounting for Stochastic Errors," *Journal of Spacecraft and Rockets*, Vol. 35, No. 5, 1998, pp. 683–689.

[13] Vinh, N., Busemann, A., and Culp, R., *Hypersonic and Planetary Entry Flight Mechanics*, Univ. of Michigan Press, Ann Arbor, MI, 1980, Chaps. 2, 3.

[14] Johnson, W., Longuski, J., and Lyons, D., "Six-Degree-of-Freedom Modeling of Semi-Autonomous Attitude Control During Aerobraking," *Journal of Spacecraft and Rockets* (to be published).

[15] Longuski, J., "Can Aerogravity-Assist Through the Venusian Atmosphere Permit a Near Radial Trajectory into the Sun?" Jet Propulsion Lab., Engineering Memorandum EM 312/82-133 (JPL Document), California Inst. of Technology, Pasadena, CA, Dec. 1982.

[16] Longuski, J., Puig-Suari, J., and Mechalas, J., "Aerobraking Tethers for the Exploration of the Solar System," *Acta Astronautica*, Vol. 35, No. 2/3, 1995, pp. 205–214.

[17] Croom, C., and Tolson, R., "Using Magellan Attitude Control Data to Study the Venusian Atmosphere and Various Spacecraft Properties," *AAS/AIAA Spaceflight Mechanics Meeting*, Vol. 87, Pt. 1, edited by J. E. Cochran Jr., C. D. Edwards Jr., S. J. Hoffman, and R. Holdaway, Univelt, San Diego, CA, 1994, pp. 451–468.

[18] Haas, B., and Schmitt, D., "Simulated Rarefied Aerodynamics of the Magellan Spacecraft During Aerobraking," AIAA Paper 93-3676, July 1993.

Color reproductions courtesy of Jet Propulsion Laboratory, California Institute of Technology.